Journal of Alloys and Compounds 480 (2009) 334–339

Contents lists available at ScienceDirect

Journal of Alloys and Compounds

journal homepage: www.elsevier.com/locate/jallcom

Influence of indium addition on structure, mechanical, thermal and electrical properties of tin–antimony based metallic alloys quenched from melt

Rizk Mostafa Shalaby

Metal Physics Laboratory, Physics Department, Faculty of Science, Mansoura University, P.O. Box 35516, Mansoura, Egypt

ARTICLE INFO

Article history:
Received 10 November 2008
Received in revised form 30 January 2009
Accepted 2 February 2009
Available online 13 February 2009

Keywords:
Solder
Soldering
Lead free
Electronic applications
Mechanical properties
Thermal properties

ABSTRACT

The melt-spinning processes of binary Sn–10 wt.% Sb and ternary Sn–10 wt.% Sb–In were analyzed using X-ray diffractometer and differential thermal analysis (DTA). The results showed that supersaturated solid solution and new intermetallic compound In_3Sn were produced during melt-spinning technique not found under equilibrium conditions. It is also found that a small amount of In addition significantly lowers the melting point of the Sn–10 wt.% Sb alloy and reduce the crystal size to ≈60 nm. Also, tin–antimony solder doped with In exhibits good mechanical properties, Vickers hardness and mechanical strength due to refined microstructure. This work was performed to study the influence of rapid solidification and indium addition on structure and properties of tin–antimony based alloys.

© 2009 Elsevier B.V. All rights reserved.

1. Introduction

Sn–Sb is one of the materials considered for replacing lead containing alloys for soldering in electronic packaging. The relatively high melting point of Sn–Sb alloy makes it suitable for high temperature applications. The antimony has the effect of imparting strength and hardness to the alloy. Formation of the intermetallic compound SbSn is possible at these levels of Sb. This phase has a cubic structure with a high hardness. To become a viable lead-free solder alternative for electronics assembly use, it is considered essential for this candidate solder to meet the following criteria: melting temperature, similar to Sn–Pb solders, particularly 63Sn–37Pb solder; adequate wetting properties to metallization used in electronics industry; physical properties no poorer then those of Sn–Pb solder; good fatigue resistance; relatively non-toxic and low cost. The modification in tin–antimony alloys have been studied [1]. They found that the results obtained by rapid cooling, compared with the slow cooling, greatly affects the structure and properties of Sn–Sb alloys. It leads to a much finer-grained structure and therefore, gives rather better mechanical strength. It also leads to the formation of new phases, not found under equilibrium conditions. Investigation of the temperature dependence of the electrical resistivity (ρ–T) of Sn–Sb alloys is carried out, using the DC four-probe method [2]. Tin–antimony alloys have been studied by many investigators [3,4]. However, papers on Sn–Sb alloys [5–8] seldom concentrate on temperature induced structural behavior of Sn–Sb melts. Moreover, according to Sn–Sb phase diagram (Fig. 1 [9]), there are two intermediate phases and extended solid solutions. Tensile, creep, and the automated ball indentation (ABI) tests on Sn–5Sb solder for mechanical property evaluation [10].

The aim of this work is to study the effects of the solidification rate and the small additions of indium on the mechanical, structure, thermal and the electrical properties of the Sn–10 wt.% Sb alloy.

2. Experimental

Five alloys of compositions Sn–10 wt.% Sb, Sn–10 wt.% Sb–0.5In, Sn–10 wt.% Sb–1.0 wt.% In, Sn–10 wt.% Sb–1.5 wt.% In and Sn–10 wt.% Sb–2.0 wt.% In have been produced by a single copper roller melt-spinning technique. Required quantities of the used metals were weighed out and melted in a porcelain crucible. After the alloys were molten, the melt was thoroughly agitated to effect homogenization. The casting was done in air at a melt temperature of 600 °C. The speed of the copper wheel was fixed at 2900 rpm; which corresponds to a linear speed of 30.4 m/s. X-ray diffraction (XRD) analysis is carried out with a Shimadzu-X-ray diffractometer (DX-30), using Cu Kα radiation with Ni filter (λ = 0.154056 nm). Differential thermal analysis (DTA) is carried out in a Shimazu DT-50 with a heating rate 10 K/min. The measurement of resistivity is carried out by the double bridge method. The Vickers microhardness number (H_v) is measured using the FM-7 microhardness tester. The elastic moduli of melt-spun ribbons were examined in an air atmosphere with a dynamic resonance method.

E-mail address: rizk1969@yahoo.co.uk.

0925-8388/$ – see front matter © 2009 Elsevier B.V. All rights reserved.
doi:10.1016/j.jallcom.2009.02.013

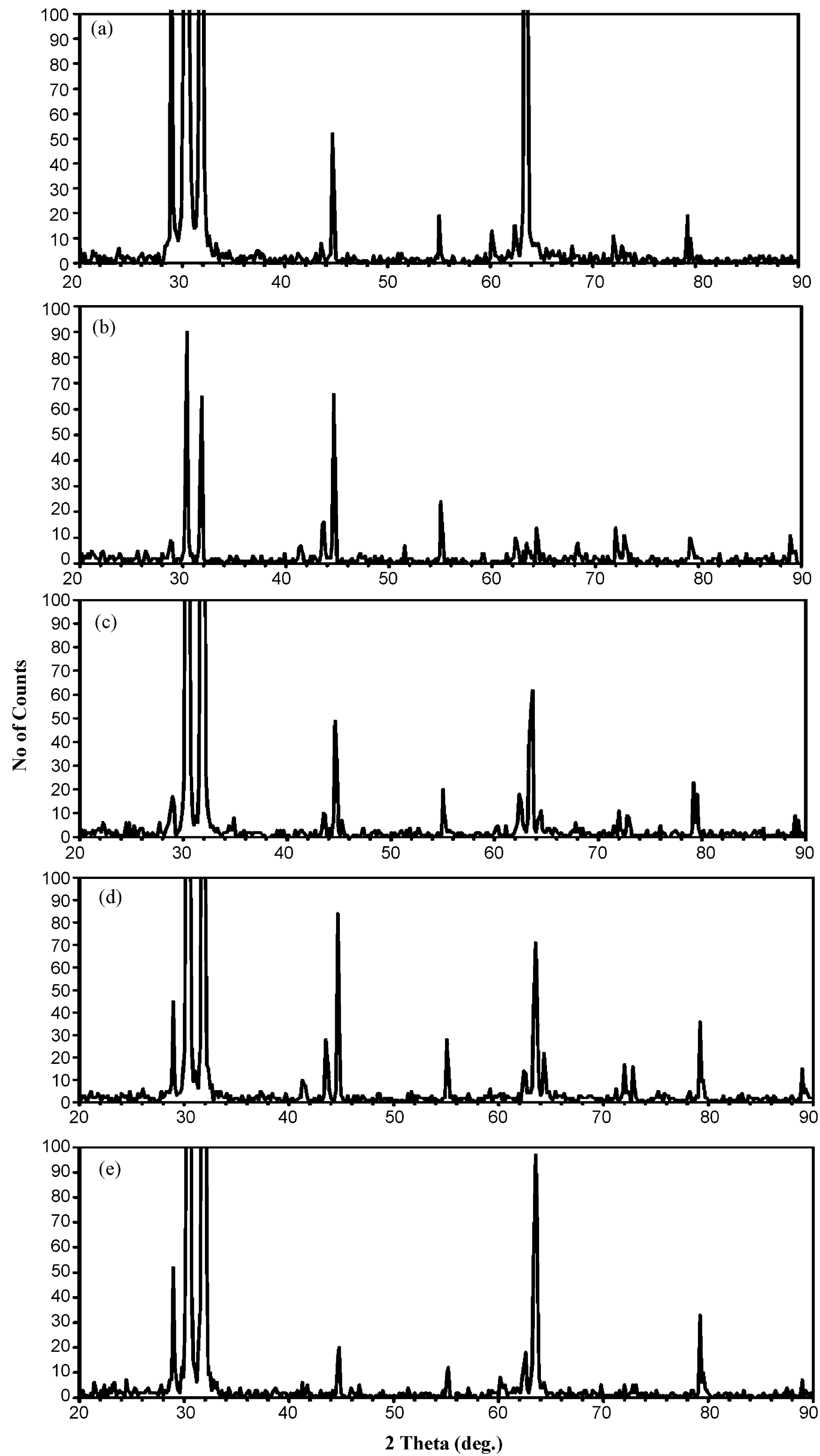

Fig. 1. The XRD patterns of as-quenched melt-spun: (a) $Sn_{90}Sb_{10}$, (b) $Sn_{89.5}Sb_{10}In_{0.5}$, (c) $Sn_{89}Sb_{10}In_{1.0}$, (d) $Sn_{88.5}Sb_{10}In_{1.5}$ and (e) $Sn_{88}Sb_{10}In_{2.0}$ alloys.

3. Results and discussion

3.1. Structure

Fig. 1 shows the XRD patterns for as-quenched melt-spun ribbons of all compositions $Sn_{90-x}Sb_{10}In_x$ ($x \geq 0$). The structure of Sn–10 wt.% Sb alloy Fig. 1a contains SnSb embedded in the Sn matrix at $2\theta = 29.10$, 41.65 and 60.36. For Sn–10 wt.% Sb–0.5 wt.% In alloy Fig. 1b, the number of peaks and intensity due to SnSb increases at $2\theta = 29.19$, 41.92, 51.81 and 60.55, Also, the pattern contains two peaks for In_3Sn at $2\theta = 79.49$ and 89.43. Also, Fig. 1c–e show that presence of SnSb and In_3Sn phases which is not normally

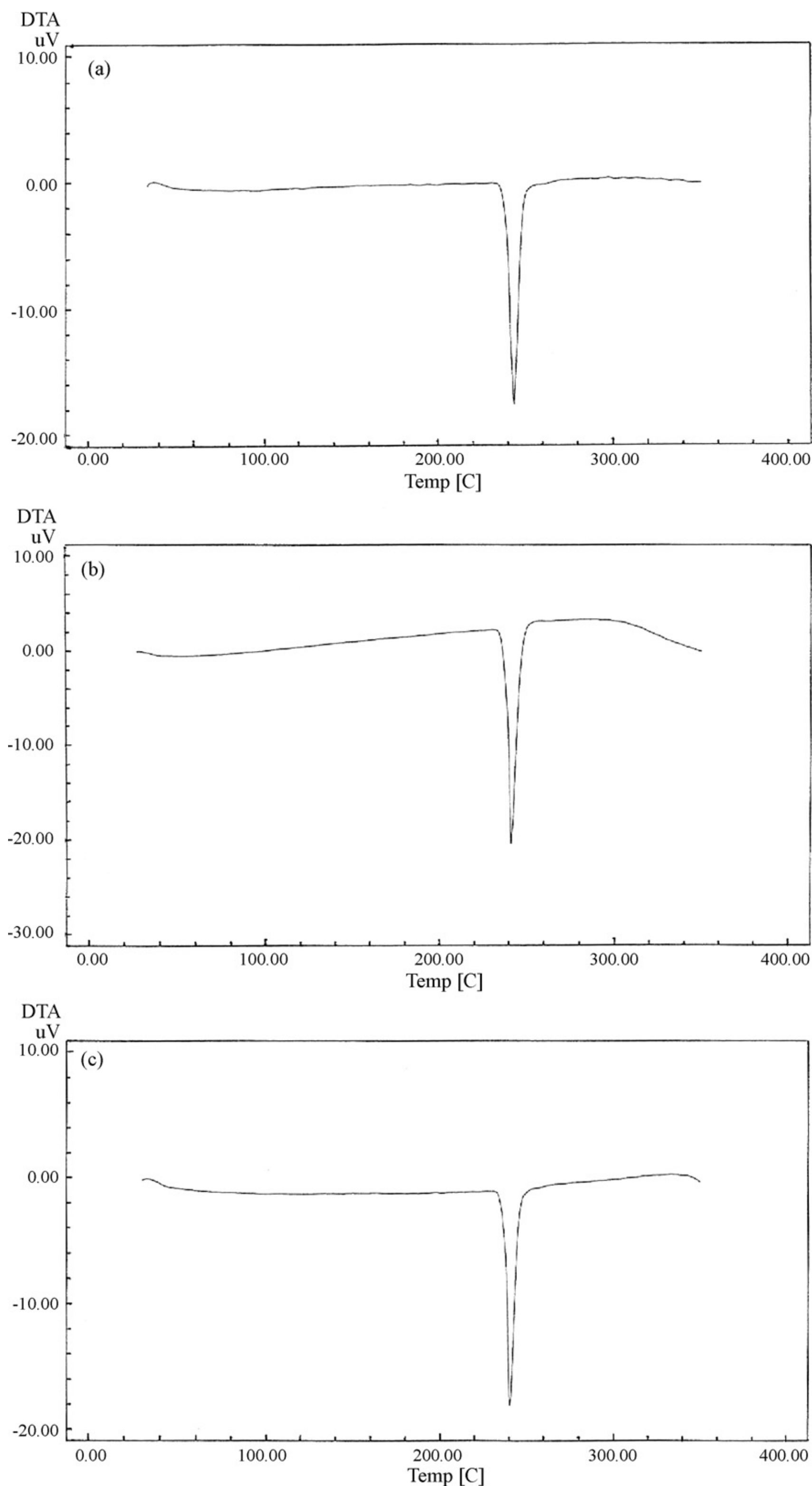

Fig. 2. Differential thermal analysis (DTA) of all melt-spun alloys: (a) $Sn_{90}Sb_{10}$, (b) $Sn_{89.5}Sb_{10}In_{0.5}$, (c) $Sn_{89}Sb_{10}In_{1.0}$, (d) $Sn_{88.5}Sb_{10}In_{1.5}$ and (e) $Sn_{88}Sb_{10}In_{2.0}$.

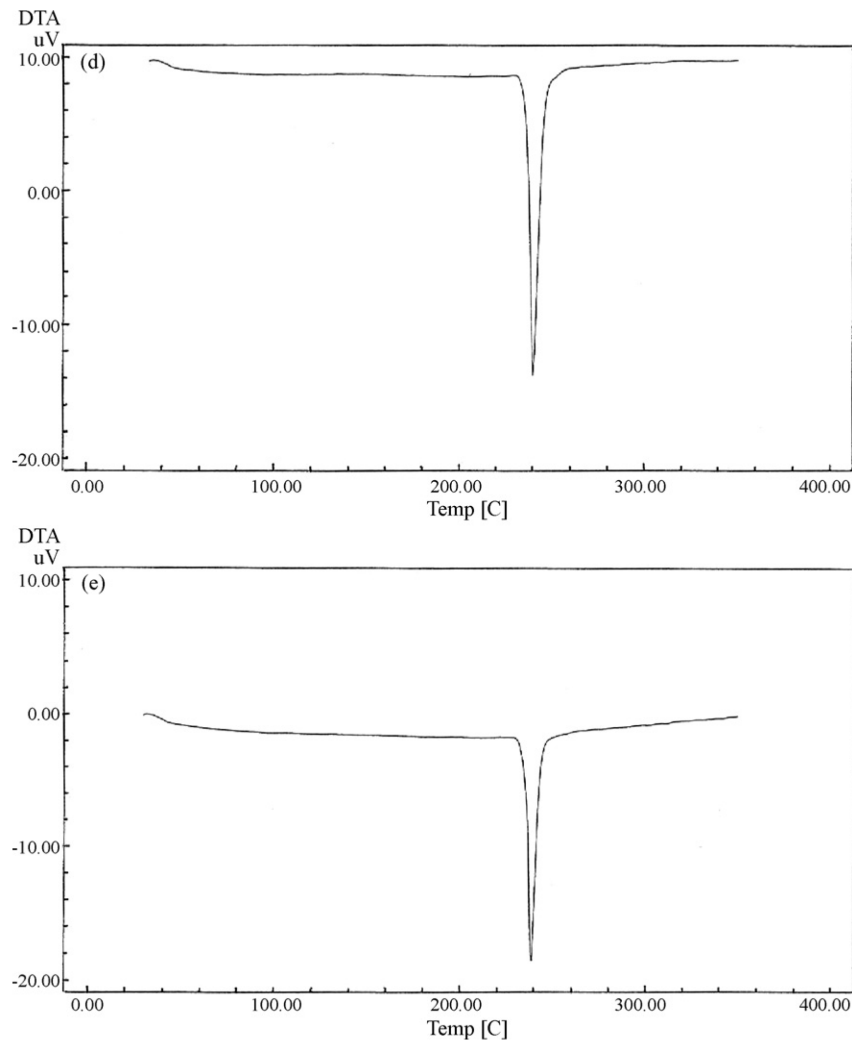

Fig. 2. (*Continued*).

obtained under equilibrium conditions. The In_3Sn compound has β-tetragonal structure. The details of the XRD analysis are shown in Table 1.

Table 1
The details of the XRD analysis.

System	Phase designation	Crystal system	Crystal size (nm)
$Sn_{90}Sb_{10}$	SbSn	Rhombohedral (Hex)	160.5
	Sn	Body centered tetragonal	182.8
$Sn_{89.5}Sb_{10}In_{0.5}$	SbSn	Rhombohedral (Hex)	130.4
	Sn	Body centered tetragonal	140.3
	In_3Sn	Tetragonal	130.2
$Sn_{89}Sb_{10}In_{1.0}$	SbSn	Rhombohedral (Hex)	118.5
	Sn	Body centered tetragonal	120.2
	In_3Sn	Tetragonal	118.5
$Sn_{88.5}Sb_{10}In_{1.5}$	SbSn	Rhombohedral (Hex)	88.5
	Sn	Body centered tetragonal	110.2
	In_3Sn	Tetragonal	86.5
$Sn_{88}Sb_{10}In_{2.0}$	SbSn	Rhombohedral (Hex)	60.3
	Sn	Body centered tetragonal	56.5
	In_3Sn	Tetragonal	66.5

3.2. Thermal analysis

The DTA curves obtained for the five alloys during heating with heating rate 10 K/min are shown in Fig. 2. The figure for all prepared alloys $Sn_{90-x}Sb_{10}In_x$ ($x \geq 0$) shows a single endothermic peak corresponding to the melting reaction. From this figure the melting point (T_m), solidus temperature (T_s), liquidus temperature (T_l), enthalpy of fusion (ΔH_f) and pasty range of these alloys were calculated and presented in Table 2. The melting point decreases continuously with indium content up to 233 °C at 2 wt.% In. This reduction may be attributed to the decrease of the crystalline size, as observed in the work of Peter et al. [11]. The enthalpy of fusion is higher

Table 2
Thermal analysis.

Alloy	T_m (°C)	ΔH_f (kJ/g)	Pasty range (°C)	Solidus temperature (°C)	Liquidus temperature (°C)
Sn–10Sb	240	56.95	20.81	232.44	253.25
Sn–10Sb–0.5In	238	73.63	22.46	230.25	252.71
Sn–10Sb–1.0In	237	51.36	22.31	227.64	249.95
Sn–10Sb–1.5In	235	73.57	29.59	224.90	254.49
Sn–10Sb–2In	233	49.40	22.22	225.91	248.13

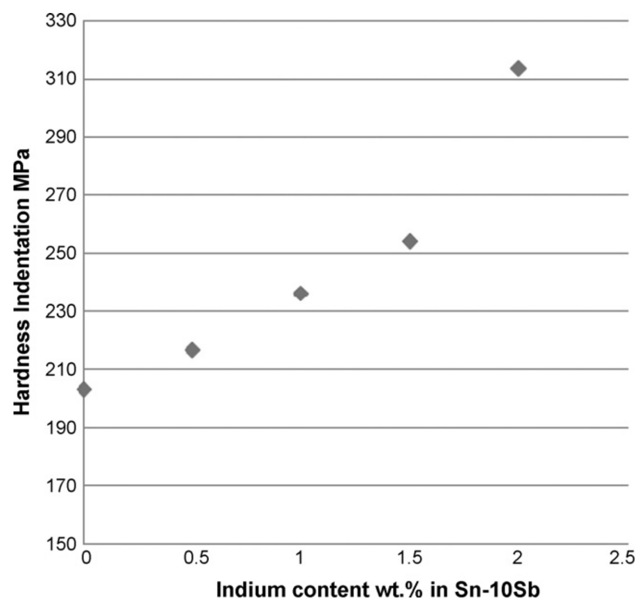

Fig. 3. The variation of H_v with indium content.

Table 3
Vickers microhardness (H_v) and yield stress (σ_y) of all prepared alloys.

Alloy	H_v (MPa)	σ_y (MPa)
Sn–10Sb	203.16	67.83
Sn–10Sb–0.5In	216.66	72.22
Sn–10Sb–1.0In	236.27	78.75
Sn–10Sb–1.5In	253.92	84.64
Sn–10Sb–2In	313.72	104.57

value for 0.5 and 1.5 wt.% indium, may be due to the indium addition and presence of intermetallic compounds. The pasty range (the solidus–liquidus distance), which is the range between the solidus and liquidus temperatures, for the eutectic alloy is equal to zero, while for the other alloys exhibits a positive increase up to 29.59 °C. The solder in this range of temperature is a semi-solid and has properties different from the solid or the liquid phases. This behavior leads to the solder left-off during solidification. In order to avoid this problem it is preferable to use a solder with very narrow pasty range.

3.3. Hardness indentation

Fig. 3 shows the variation of microhardness H_v with Indium content for constant applied load 10 gf dwell time 5 s. For Sn–10Sb, H_v has the lowest value 203.49 MPa. After addition, the indium at 0.5, 1.0, 1.5 and 2.0 wt.%, the H_v increases up to reach 313.72 MPa at 2.0-wt.% Indium. This is attributed to the presence of more intermetallic compounds such as SnSb and In_3Sn and refinement the crystal size. Also, this behavior can be explained in terms of the alloy structure and resulting properties. With this relatively high amount of antimony, a large amount of the hard SbSn phase is likely present. These SbSn cubes can act as crack initiation sites and eventually lead to failures. Therefore, the high strength which the high antimony content imparts may prove to be too stiff for microelectronics applications where compliance to shear stresses is a requirement. Table 3 shows the H_v and yield stress (σ_y) for more the as-quenched melt-spun $Sn_{90-x}Sb_{10}In_x$ alloys.

Table 4
Electrical resistivity at room temperature of all prepared alloys with and without indium.

Alloy	ρ (μΩ cm)
Sn–10Sb	26.25 ± 2.1
Sn–10Sb–0.5In	27.55 ± 1.7
Sn–10Sb–1.0In	29.33 ± 1.5
Sn–10Sb–1.5In	30.25 ± 1.6
Sn–10Sb–2In	32.37 ± 1.8

3.4. Electrical properties

In microelectronic devices the solder serves as an electrical interconnection. Therefore, in most microelectronic applications the resistivity of the solder interconnects should be so thin that it does not affect the functionality of the circuit. The electrical resistivity (ρ) of as-quenched melt-spun alloys is measured at room temperature and the results are shown in Table 4. The increase in the resistivity after addition indium up to 2 wt.% is due to the formation of SnSb and In_3Sn intermetallic compound which acts hard inclusions in the soft matrix and rate of cooling [12].

3.5. Mechanical properties

The strength of the material is limited by the atomic bonding forces, which are reflected macroscopically by the elastic constants. Table 5 shows the values of the elastic moduli and Lame's constant of all prepared alloys calculated from the resonance curve obtained by the dynamic resonance circuit after determination of the resonance frequency. It shows an increase of the Elastic modulus to the maximum value of 55 GPa at 2 wt.% In. It is due to presence of hard intermetallic compounds, which act as hard inclusions in the soft matrix.

Values of Shear modulus (G), Bulk modulus (B) and Lame's constant (λ) were calculated using standard equations:

$$G = \frac{E}{2(1+\nu)} \quad B = \frac{E}{3(1-2\nu)}, \quad \text{and} \quad \lambda = \frac{\nu E}{(1+\nu)(1-2\nu)}$$

The tensile fracture strength (σ_f), tensile fracture strain ($\varepsilon_{t,f} = \sigma_f/E$), compressive yield strain ($\varepsilon_{c,y} = H_v/3E$) and compressive yield strength ($\sigma_{c,y} = H_v/3$) are shown in Table 5. It is found that the tensile fracture strength, compressive yield strength increasing with Indium content. This may be due to high performance metal alloys are never single phase but generally consists of a matrix interspersed by areas of second phase material or intermetallic phases such as SnSb or In_3Sn.

Table 5
Mechanical properties of $Sn_{90-x}Sb_{10}In_x$ melt-spun alloys.

Alloy	Young's modulus E (GPa)	Shear modulus G (GPa)	Bulk modulus B (GPa)	Lame's constant λ (GPa)	σ_f (GPa)	$\varepsilon_{c,y}$ (10^{-3})	$\varepsilon_{t,f}$
Sn–10Sb	52.25	19.49	54.42	41.42	10.21	1.29	0.195
Sn–10Sb–0.5In	58.78	21.73	61.22	46.60	10.84	1.22	0.184
Sn–10Sb–1.0In	59.89	22.34	62.38	47.78	10.94	1.31	0.182
Sn–10Sb–1.5In	62.64	23.37	65.25	49.66	11.19	1.35	0.178
Sn–10Sb–2In	65.22	24.33	67.93	51.71	11.42	1.60	0.175

4. Conclusions

From previous studies it is concluded that:

Rapid solidification and the addition of In to Sn–10 wt.% Sb lead to the formation the intermetallic compound In_3Sn which is not normally obtained under equilibrium conditions. Also, the addition of indium to Sn–10 wt.% Sb alloy increases the hardness, elastic moduli; yield stress and delay the fracture strength by refine the effective crystal size to about 60 nm at 2 wt.% In. Also, the melting points and pasty range of these solders are desirable by comparison with Pb–Sn solder alloys. On the other hand adding indium to the binary alloy (Sn–10 wt.% Sb) causes increase in electrical resistivity due to formation of intermetallic compound In_3Sn and SnSb which act as scattering centers for conduction electrons.

References

[1] M. Kamal, A. Abdel-Salam, J.C. Pieri, J. Mater. Sci. 19 (1984) 3880–3886.
[2] Fang-Qiu Zu, Rong-Rong Shen, Yun Xi, Xian-Fen Li, Guo-Hua Ding, Hai-Ming Liu, J. Phys.: Condens. Matter 18 (2006) 2817–2823.
[3] M.L. Huang, C.M.L. Wu, J.K.L. Lai, L. Wang, F.G. Wang, J. Mater. Sci.: Mater. Electron. 11 (9) (2000) 57–67.
[4] Sinn-Wen Chen, Po-Yin Chen, Chao-Hong Wang, J. Electron. Mater. 35 (4) (2006) 1982–1985.
[5] V. Vassiliev, M. Lelaurain, J. Hertz, J. Alloys Compd. 247 (1997) 223–233.
[6] P.F. Qi, H.B. Zhang, S.L. Gao, Q.J. Zhai, J. Shanghai Univ. 9 (2005) 74–77.
[7] E. Dashjav, Kleinke H, J. Solid State Chem. 176 (2003) 329–337.
[8] R. Koivula, R. Harjula, J. Lehto, Micropor. Mesopor. Mater. 55 (2002) 231–238.
[9] E. Dichi, A. Wojakowska, B. Legendre, J. Alloys Compd. 320 (2001) 218–223.
[10] K.L. Murty, R.K. Mahidhara, Fahmy M. Haggag, J. Electron. Mater. 26 (7) (1997) 839–846.
[11] A. Peters, B. Chung, C. Cohen, Appl. Phys. Lett. 71 (1997) 2391.
[12] R.M. Shalaby, J. Mater. Sci.: Mater. Electron. 16 (2005) 187–191.